# Application of the optical fiber to generation and measurement of low-phase-noise microwaves

K. Volyanskiy,[*] J. Cussey,[†] H. Tavernier, P. Salzenstein, G. Sauvage,[‡] L. Larger, and E. Rubiola[§]

*FEMTO-ST Institute, UMR 6174 CNRS and Université de Franche Comté, Besançon, France*

## I. INTRODUCTION

This article describes a series of experiences related to the generation and to the measurement of low-phase-noise microwave signals using the optical fiber as a delay unit. The main reasons to use the optical fiber, together with laser, intensity modulator and photodetector, to implement a microwave delay are (1) the long achievable delay, due to the low loss (0.2 dB/km typical) of the fiber, (2) the wide bandwidth of the delay, (3) the low background noise, and (4) the low thermal sensitivity of the delay. The latter has a typical value of $6.85 \times 10^{-6}$/K, a factor of 10 better than the sapphire dielectric cavity. These features enables the implementation of high spectral purity oscillators and of high-sensitivity instruments for the measurements of phase noise. In both cases, the optical bandwidth turns into wide-range microwave tunability at virtually no cost in terms of phase noise.

The scientific motivations are the same of [1] for the oscillator, and of [2] for the instruments. This work adds to the available knowledge a considerable amount of engineering, accurate calibration, the use of the cross-spectrum technique to reduce the instrument background (after the pioneering article [3] and our early implementation [4]), the phase-noise model of the oscillator, and the experimental verification of the oscillator model.

## II. MATHEMATICAL BACKGROUND

### A. Phase noise

Phase noise is a well established subject, clearly explained in numerous classical references, among which we prefer [5–8] and [9, vol. 1, chap. 2]. Thus, the short summary we gives aims only at recalling the vocabulary.

The quasi-perfect sinusoidal signal of frequency $\nu_0$, of random amplitude fluctuation $\alpha(t)$, and of random phase fluctuation $\varphi(t)$ is

$$v(t) = [1 + \alpha(t)] \cos [2\pi\nu_0 t + \varphi(t)] . \quad (1)$$

We may need that $|\alpha(t)| \ll 1$ and $|\varphi(t)| \ll 1$ during the measurement. Phase noise is generally measured

————————

[*]Joint affiliation with the St. Petersburg State University of Aerospace Instrumentation.
[†]Now with Smart Quantum, Lannion & Besançon, France.
[‡]Aeroflex, Paris, France.; URL: http://www.aeroflex.com
[§]Electronic address: rubiola@femto-st.fr; URL: http://rubiola.org

as the average PSD (power spectral density) $S_\varphi(f)$

$$S_\varphi(f) = \left\langle |\Phi(jf)\}|^2 \right\rangle_m \quad \text{(avg, } m \text{ spectra)}, \quad (2)$$

where $\Phi(jf)$ is the Fourier transform of $\varphi(t)$. In experiments, the single-sided PSD is preferred to the two-sided PSD because the negative frequencies are redundant. Accordingly, we use $S_\varphi(f)$ as the single-sided PSD.

A model that has been found useful to describe accurately the phase noise of oscillator and components is the power law

$$S_\varphi(f) = \sum_{n=-4}^{0} b_i f^n \quad \text{(power law)}. \quad (3)$$

This model relies on the fact that white ($f^0$) and flicker ($1/f$) noises exist per-se, and that phase integration ($\times 1/f^2$) is present in oscillators. If needed, the model can be extended to steeper processes, that is, $n < -4$.

A quantity often used is the fractional frequency fluctuation $y(t) = \dot{\varphi}(t)/2\pi\nu_0$. The spectrum $S_y(f)$ is

$$S_y(f) = \frac{f^2}{\nu_0^2} S_\varphi(f) = \sum_{n=-2}^{2} h_i f^n . \quad (4)$$

Another tool often used is the Allan variance $\sigma_y^2(\tau)$. Notice that the measurement time $\tau$ is *not* the delay of the line (Sec. II C). We will change symbols if needed. For the most useful frequency-noise processes, the relation between $\sigma_y^2(\tau)$ and $S_y(f)$ is

$$\sigma_y^2(\tau) = \begin{cases} \dfrac{h_0}{2\tau} & \text{white freq. noise} \\[2mm] h_{-1}\, 2\ln(2) & \text{flicker of frequency} \\[2mm] h_{-2}\, \dfrac{(2\pi)^2}{6}\, \tau & \text{random walk of freq.} \end{cases} \quad (5)$$

### B. Cross-spectrum method

The measured noise PSD includes the device under test (DUT) noise and the instrument background. Improved sensitivity is obtained using a cross-spectrum method, in which two equal instruments measure simultaneously the same DUT. A short digression is given in this Section. The mathematical details and the in-depth analysis of the experimental method are reported in [10], in these Proceedings.

Let $a(t)$ and $b(t)$ the background of the two instruments, and $c(t)$ the common noise. By definition,

$a(t)$, $b(t)$ and $c(t)$ are statistically independent. The two outputs are

$$x(t) = c(t) + a(t) \tag{6}$$
$$y(t) = c(t) + b(t) \ . \tag{7}$$

We denote the Fourier transform with the uppercase of the time-domain function, thus $a(t) \leftrightarrow A(jf)$, etc. The cross-spectrum averaged on $m$ measures is

$$\begin{aligned}
S_{yx}(f) &= \langle YX^* \rangle_m \\
&= \langle \{[C+A] \times [C+B]^* \rangle_m \\
&= \langle CC^* \rangle_m + \langle CB^* \rangle_m + \langle AC^* \rangle_m + \langle AB^* \rangle_m \\
&= S_c(f) + O(\sqrt{1/m}) \ , \tag{8}
\end{aligned}$$

where $O(\ )$ means 'order of.' Owing to statistical independence, the cross terms decrease as $\sqrt{1/m}$.

The measurement and the assessment of the instrument background go as follows.

1. With no DUT noise, and maintaining the hypothesis of statistical independence of the two channels, it holds that $c = 0$. The *statistical limit* of the measurement is

$$S_{yx}(f) \approx \sqrt{\frac{1}{m} S_a(f) S_b(f)} \qquad \text{(stat. limit).} \tag{9}$$

Accordingly, a 5 dB improvement on the single-channel noise costs a factor of 10 in averaging, thus in measurement time.

2. Breaking the hypothesis of the statistical independence of the two channels, we interpret $c$ as the correlated noise of the instrument, due to environment, crosstalk, etc. Thus, still at zero DUT noise, we get the *hardware limit* of the instrument sensitivity

$$S_{yx}(f) = S_{c''}(f) \qquad \text{(hardware limit).} \tag{10}$$

3. Now we introduce the DUT noise. If (i) $m$ is large enough for the statistical limit to be negligible, and (ii) the background is negligible as compared to the DUT noise, the cross spectrum gives the *DUT noise*

$$S_{yx}(f) = S_c(f) \simeq S_{c'}(f) \qquad \text{(DUT meas.).} \tag{11}$$

This is the regular use of the instrument.

### C. Delay line theory

Delaying the signal $v(t)$ by $\tau$, all time-varying parameters of $v(t)$ are also delayed by $\tau$, thus the phase fluctuation $\varphi(t)$ turns into $\varphi(t-\tau)$. By virtue of the time-shift theorem, the Fourier transform of $\varphi(t-\tau)$ is $e^{-j2\pi\tau f}\Phi(jf)$. This enables the measurement of the oscillator phase noise $\varphi(t)$ by observing the difference $\theta(t) = \varphi(t) - \varphi(t-\tau)$. By inspection on Fig. 1, it holds that
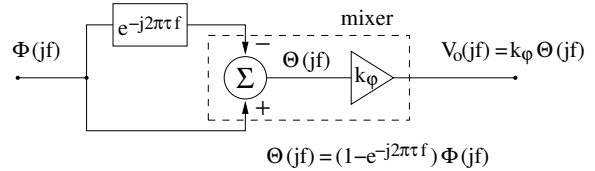
$$\Theta(jf) = H(jf)\,\Phi(jf) \ , \tag{12}$$



Figure 1: Basic delay-line phase noise measurement.
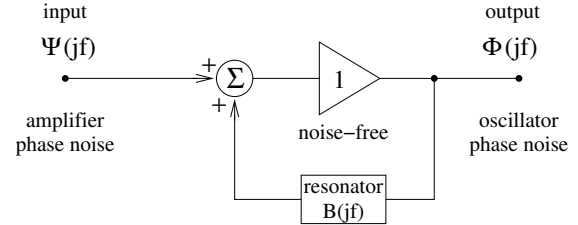


Figure 2: Oscillator phase-noise model.

where $H(jf) = 1 - e^{-j2\pi\tau f}$, and consequently

$$S_\theta(f) = |H(jf)|^2 S_\varphi(f) \tag{13}$$
$$|H(jf)|^2 = 4\sin^2(\pi f \tau) \tag{14}$$

The oscillator noise $S_\varphi(f)$ is inferred by unapplying $|H(jf)|^2$ to the measured output $S_\theta(f)$. In actual measurements it is important to keep the measurement and the use of $|H(jf)|^2$ separated because detecting most of the experimental mistakes on $S_\theta(f)$ is significantly easier than on $S_\varphi(f)$. For $f \to 0$, it holds $|H(jf)|^2 \sim f^2$. Fortunately, high slope processes such as frequency flicker ($S_\varphi(f) = b_{-3}/f^3$) dominate in this region, which compensates $|H(jf)|^2$. The phase noise measurement is therefore possible. The function $|H(jf)|^2$ has a series of zeros, in the vicinity of which the experimental results are not useful. In practice, the first zero sets the maximum measurement bandwidth to $0.9/\tau$, as discussed in [2].

### D. Oscillator phase noise

The oscillator consists of an amplifier of gain $A$ (constant) and of a feedback path of transfer function $\beta(jf)$ in closed loop. The function $\beta(jf)$ selects the oscillation frequency, while the gain $A$ compensates for the feedback loss. This general model is independent of the nature of the amplifier and of the frequency selector. We assume that the Barkhausen condition $|A\beta(jf)| = 1$ for stationary oscillation is verified at the carrier frequency $\nu_0$ by saturation in the amplifier or by some other gain-control mechanism. Under this hypothesis, the phase noise is modeled by the scheme shown in Fig. 3, in which all signals are *the phases of the oscillator loop*. The main reason for describing the oscillator in this way is that we get rid of the non-linearity, pushing it in the loop-gain stabilization. The ideal amplifier 'repeats' the phase of the input, for it has a gain of one (exact) in the phase-noise model. The real amplifier introduces the random phase $\psi(t) \leftrightarrow \Psi(jf)$ in the loop.

In this representation, the phase noise is always additive noise, regardless of the physical mechanism involved. This eliminates the mathematical difficulty inherent in the parametric nature of flicker noise and of the noise originated from the environment fluctuations. The feedback path is described by the transfer function $B(jf)$ of the phase perturbation.

In the case of the *delay-line oscillator*, the feedback path is a delay line of delay $\tau_d$ followed by a selector filter. The delay line enables oscillation at any frequency multiple of $1/\tau_d$, with no preference. The filter is necessary to select one of those frequencies, denoted with $\nu_0$. Implementing the selector as a resonator of relaxation time $\tau_f$, the phase-perturbation response of the feedback path is

$$B(jf) = \frac{e^{-j2\pi\tau_d f}}{1 + j2\pi\tau_f f} \ . \tag{15}$$

Neglecting the difference between natural frequency and oscillation frequency, the relaxation time is related to the quality factor $Q$ by $\tau_f = Q/\pi\nu_0$ We assume that all the phase perturbations in the loop are collected in the random function $\psi(t) \leftrightarrow \Psi(jf)$, regardless of the physical origin (amplifier, photodetector, optical fiber, etc.). Denoting with $\varphi(t) \leftrightarrow \Phi(jf)$ the oscillator output phase, the oscillator is described by the phase-perturbation transfer function

$$H(jf) = \frac{\Phi(jf)}{\Psi(jf)} \ . \tag{16}$$

Using the basic equations of feedback, the oscillator transfer function is

$$H(jf) = \frac{1}{1 - B(jf)} \ , \tag{17}$$

thus,

$$H(jf) = \frac{1 + j2\pi\tau_f f}{1 + j2\pi\tau_f f + e^{-j2\pi\tau_d f}} \ . \tag{18}$$

All the mathematical details of Eq. (18) and its proof are available in the book [11] (forthcoming). The result is confirmed using the phase diffusion and the formalism of stochastic processes [12].

Figure 3 shows an example of oscillator phase noise calculated using $S_\varphi(f) = |H(jf)|^2 S_\psi(f)$, after introducing white and flicker phase noise in the loop. Interestingly, the bandwidth of the noise peaks is extremely narrow, in the Hertz or sub-Hertz range. Consequently, the measurement shows the resolution of the instrument, or of the plot, instead of the true peak width. With uniform instrument bandwidth, the peak height follows the law $S_\varphi(f) \sim 1/f^4$ ($-40$ dB/decade). Eliyahu [13, Sec. IV] reports having observed a discrepancy by a factor $f$ (30 dB/decade). Yet, this reference does not describe the measurement sufficiently in depth to understand wether the observed law is the true distribution of the oscillator noise peaks or it results from an instrument effect.
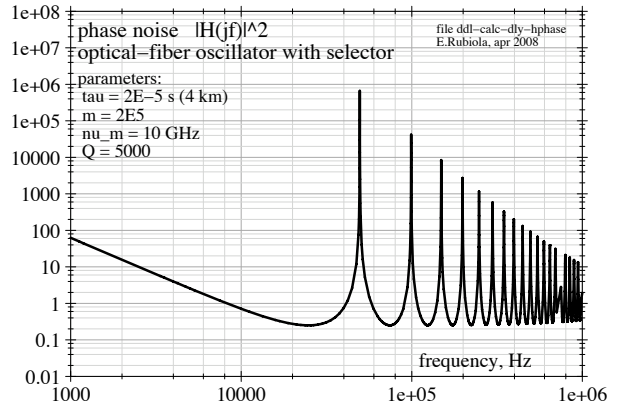


Figure 3: Oscillator phase-noise transfer function.

## III. OPTICAL-FIBER DELAY UNIT

### A. Design strategy

Figure 4 shows the optical-fiber microwave delay unit. For practical reasons, we have to use components available off-the-shelf, mainly intended for telecommunications applications. The microwave components limit the frequency range to 4–5 GHz around the central frequency of 10 GHz. The system is designed for low noise and for high stability of the delay, as discussed underneath.

The optical fiber is a Corning SMF-28 wound on a cylinder of 15 cm diameter and 2 cm heigth. We used 2 km (10 $\mu$s) and 4 km (20 $\mu$s) length in most experiments, and sometimes shorter fibers. The spool is enclosed in a 5 mm thick Duralumin cylinder thermally insulated from the environment by some 3 cm plastic foam. The cylinder is temperature stabilized at room temperature within a fraction of a milliKelvin with a PID control built in our laboratory and set with the well-known Ziegler-Nichols method. The advantage of the temperature control vs. a passive time constant, i.e., large metal mass and thermal insulator, is still questionable. For short-term fluctuations (100 ms or less), the passive stabilization would certainly be preferable because it does not suffer from the noise inherent in the control. On the other hand, we need to keep the delay and the phase relationships stable for the duration of the correlation measurements, which last up to one day. In the two-channel scheme (Section IV), the control has the additional virtue to reduce the correlated part of the fluctuations induced by the environment.

The light source is a semiconductor CATV laser, temperature controlled and powered with a low-noise current source. This choice is partially motivated by the need of low RIN (relative intensity noise) at a reasonable simplicity and cost. The RIN turns into AM noise of the detected microwave signal, which pollutes the phase noise measurements. During the past two years we used both 1.32 $\mu$m and 1.55 $\mu$m wavelength lasers. The 1.55 $\mu$m wavelength is the best choice for the low attenuation of the fiber. On
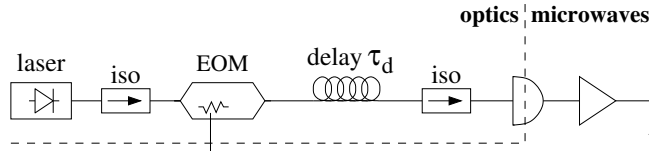
Figure 4: Optical-fiber delay unit.

the other hand, 1.3 $\mu$m wavelength is advantageous in that the dispersion of the SMF-28 fiber goes to zero at 1.311 $\mu$m, which virtually eliminates the effect of the laser frequency noise in the vicinity of that wavelength. For reference, the dispersion of the SMF-28 fiber is of 17 ps/nm/km at 1.55 $\mu$m. If a laser has a spectral width of 10 MHz ($5.8\times10^{-5}$ nm), the dispersion produces a delay fluctuation of $2\times10^{-15}$ s rms after 2 km optical fiber, which is equivalent to $1.2\times10^{-4}$ rad. Of course, this is white noise, integrated over the bandwidth. The frequency flicker of one of our lasers, converted into Allan deviation, is $\sigma_y(\tau) = 4\times10^{-10}$. This preliminary result — to be confirmed — indicates that the laser frequency stability is of less than 100 kHz (flicker floor). Thus, the laser frequency-noise contribution seems to be lower than other noises. At present time we have only a weak preference for the 1.55 $\mu$m CATV lasers, based only the more progressed technology available at this wavelength, and after comparing empirically the effect several lasers on the phase noise spectra.

Choosing the intensity-modulation method, we discarded a priori the direct modulation of the laser because the laser threshold, inherently, enhances the phases noise of the microwave signal. Thus, we opted for a MAch-Zehnder (MZ) electro-optic modulator (EOM). Other modulators, for example based on the acousto-optic effect, are not suitable to microwave modulation frequencies. We choose an EOM having low half-wave voltage ($V_\pi \simeq 3.9$ V), so that the maximum modulation is achieved with no more than 50 mW (+17 dBm) microwave power. This choice is important for stability of the half-transparency bias point because the LiNbO$_3$ is highly sensitive to temperature, thus to power and to thermal gradients. The available EOM has a low-frequency photodetector at the unused output port of the Mach-Zehnder interferometer, with which we hope to stabilize the bias point.

For low noise at microwave frequencies, the photodetector can only be a InGaAs p-i-n diode operated in strong reverse-bias conditions, thus a photoconductor. Reverse bias is necessary for high speed, as it reduces the capacitance. The need for low noise excludes some other detectors, like the avalanche diode. In our case, the photodetectors loaded to a resistor are preferable to the (more modern) photodetectors with integrated transconductance amplifier because of the possibility to choose a low flicker external amplifier.

## B. Output power and white noise

Using the subscript $\mu$ for microwave and $\lambda$ for light, and the overline for the time-average, the modulated optical power at the output of the EOM is

$$P_\lambda(t) = \overline{P}_\lambda \left[1 + \mathrm{m}\cos(2\pi\nu_\mu t)\right] \qquad (19)$$

where the modulation index m is

$$\mathrm{m} = 2J_1\left(\frac{\pi V_p}{V_\pi}\right) , \qquad (20)$$

$J_1(\ )$ is the 1st order Bessel function, $V_p$ is the microwave peak voltage, and $V_\pi$ is the modulator half-wave voltage. Equation (20) originates from the sinusoidal nature of the MZ EOM modulation transfer function, with sinusoidal input. The harmonics at frequency $n\nu_\mu$, integer $n \geq 2$, fall beyond the microwave bandwidth, thus they are discarded. Though the maximum modulation index is m = 1.164, occurring at $V_p = 0.586V_\pi$, the practical values are of 0.8–1.

The detected photocurrent is $i(t) = \rho P_\lambda(t)$, where $\rho$ is the detector responsivity. Assuming a quantum efficiency of 0.6, the responsivity is $\rho \approx 0.75$ A/W at 1.55 $\mu$m wavelength, and $\rho \approx 0.64$ A/W at 1.32 $\mu$m. The dc component of the detected current is $i_{\mathrm{dc}} = \rho\overline{P}_\lambda$. The microwave power at the detector output is

$$P_\mu = \frac{1}{2}\mathrm{m}^2 R_0 \rho^2 \overline{P}_\lambda^2 \qquad \text{(detector output)}, \qquad (21)$$

where $R_0 = 50\ \Omega$ is the load resistance.

The white noise at the input of the amplifier is

$$N = FkT_0 + 2qR_0\rho\overline{P}_\lambda \qquad \text{(white noise)} , \qquad (22)$$

where $F$ is the amplifier noise figure and $kT_0$ is the thermal energy at room temperature. The first term of (22) is the noise of the amplifier, and the second term is the shot noise. The white phase noise is, by definition [Eq. (3)], $S_\theta(f) = b_0$, constant vs. frequency (with the instrument noise, we use $\theta$ instead of $\varphi$). Using $S_\theta(f) = N/P_\mu$, we get the *white phase noise*

$$b_0 = \frac{2}{\mathrm{m}^2}\left[\frac{FkT_0}{R_0}\frac{1}{\rho^2\overline{P}_\lambda^2} + \frac{2q}{\rho\overline{P}_\lambda}\right] . \qquad (23)$$

Interestingly, the noise floor is proportional to $(\overline{P}_\lambda)^{-2}$ at low power, and to $(\overline{P}_\lambda)^{-1}$ above the threshold power

$$P_{\lambda,t} = \frac{Fk_BT_0}{R_0}\frac{1}{2\rho q} \qquad \text{(threshold power)} \qquad (24)$$
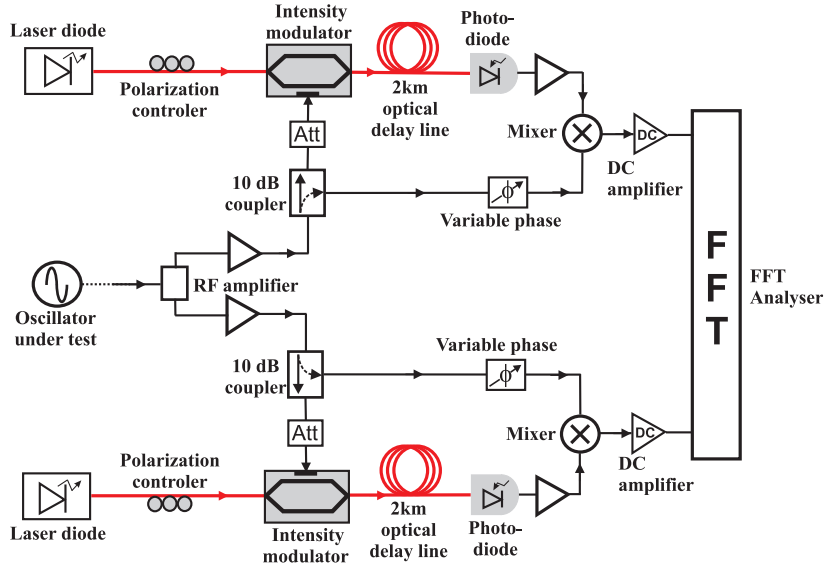
Figure 5: Scheme of the dual-channel instrument.

For example, taking $\rho = 0.75$ A/W and $F = 5$ (SiGe parallel amplifier), we get a threshold power of 1.7 mW, at which the noise floor is $b_0 \simeq 10^{-15}$ rad²/Hz ($-150$ dBrad²/Hz).

### C.   Flicker noise

Close-in flickering, which appears as phase noise and amplitude noise with PSD proportional to $1/f$, result from the near-dc $1/f$ noise up-converted by non-linearity or by a parametric modulation process. This is made evident by two simple facts:

1. The flicker noise is always present in the dc bias of the electronic devices.

2. In the absence of a carrier the microwave spectrum at the output of a device is locally white, i.e. nearly constant in a wide frequency range.

Of course, there is no reason for $1/f$ noise to show up at an arbitrary frequency, if not brought there by a carrier. Assuming that the phase modulation is approximately linear unless the carrier is so strong to shift the device dc bias, this description yields naturally to two basic rules:

1. The $1/f$ phase-noise coefficient $b_{-1}$ is independent of the carrier power.

2. Cascading two or more devices, the $1/f$ phase-noise coefficients $b_{-1}$ add up, regardless of the device order in the chain

These amazing rule contradicts the Friis formula [14], stating that the noise of each stage referred to the input of a chain is divided by the gain of the preceding stages, and consequently the first stage gives the main contribution to the total noise. Of course *the Friis formula does not apply to parametric noise.*

Experimental observation on *amplifiers* [15–17] suggest that different amplifiers based on a given technology tend to have about the same $b_{-1}$ coefficient in the power-law (3), and that $b_{-1}$ is nearly constant in a wide range of carrier frequency and power. Our independent observations confirm that the $1/f$ phase noise of a given amplifier is independent of power in a wide range [18], [19], [11, Chapter 2]. For example, $b_{-1}$ of a commercial amplifier (Microwave Solutions MSH6545502) that we measured at 9.9 GHz is between $1.25 \times 10^{-11}$ and $2 \times 10^{-11}$ from 300 $\mu$W to 80 mW of output power. Similarly, the $1/f$ noise plots of a LNPT32 SiGe amplifier measured between 32 $\mu$W ($-15$ dBm) and 1 mW (0 dBm) in 5 dB steps overlap perfectly.

In summary, the typical phase flickering $b_{-1}$ of a "good" microwave amplifier is between $10^{-10}$ and $10^{-12}$ rad²/Hz ($-100$ to $-120$ dBrad²/Hz) for the GaAs HBTs, and between $10^{-12}$ and $10^{-13}$ rad²/Hz ($-120$ to $-130$ dBrad²/Hz) for the SiGe transistors.

The microwave *photodetector* contributes with its $1/f$ fluctuations, in addition to white noise. The measurement of these $1/f$ fluctuations is a challenging experimental problem, which has been tackled at the JPL only, independently by two experimentalists [20–22]. These articles indicate that the typical flicker coefficient of a InGaAs p-i-n photodetector is of $10^{-12}$ rad²/Hz ($-120$ dBrad²/Hz).

Microwave variable attenuators and variable phase shifters can be necessary, for example to tune the oscillator frequency or to set the quadrature condition in the instrument (Section IV). Our early measurements [23] indicate that the $1/f$ phase noise coefficient $b_{-1}$ of these components is in the range of $10^{-15}$ rad²/Hz ($-150$ dBrad²/Hz), which is negligible as compared to the amplifiers and to the photodetectors.

Additional sources of noise are the EOM, the laser amplified spontaneous emission, and the noise of the optical pump (Ref. [24], Sec. 10 and Appendix C). As theory provide no indications about these effects, a pragmatic approach is necessary, which consists of

measuring the total noise of the microwave delay unit in different configurations.

## IV. DUAL-DELAY PHASE NOISE MEASUREMENT

Figure 5 shows the scheme of the instrument. However the scheme is similar to other ones published previously ([3, Fig. 6], [4, Fig. 1]), and based on the ideas published in [2], this version includes a large amount of engineering and a substantial progress in understanding $1/f$ noise.

The instrument consists of two equal and fully independent channels that measure the oscillator by comparing its phase to a delayed copy. The single-channel noise is removed using the cross-spectrum method [Eq. (11)] before calculating the oscillator noise $S_\varphi(f)$ with Eq. (14).

Looking at one channel, we observe that the microwave signal is split into two branches *before* the EOM, so that the long branch consists of modulator, optical fiber (delay $\tau$), photodetector and microwave amplifier, while the short branch is a microwave path of negligible length. This differs from the first single-channel instrument [2, Fig. 7], in which the signal was split at the *output* of the EOM. Of course, removing the photodetector and the microwave amplifier from the short branch yields lower noise, and in turn faster convergence to the correlation algorithm. Additionally, lower laser power is needed. A further, yet minor, reason is that our experience shows that the noise of a Wilkinson microwave power splitter, shared by the two channels, is negligible for our purposes [25, 26]; conversely, we have no first-hand knowledge in the case of an optical power splitter. The price to pay for the fully-microwave short branch is that we no longer have an optical input, so we are no longer able to measure the noise of microwave-modulated light beams.

Trading off with the available components, we had to use both SiGe amplifiers and GaAs amplifiers, using the GaAs as the EOM drivers. After fact, we know that this is not necessarily the best choice.

### A. Mixer Noise

When the mixer is used as a phase-to-voltage converter, saturated at both inputs, its white noise is chiefly the noise of the output amplifier divided by the conversion gain $k_\varphi$. Assuming that the amplifier noise is $1.6 \text{ nV}/\sqrt{\text{Hz}}$ (our low-flicker amplifiers input-terminated to $50 \ \Omega$ [27]) and that $k_\varphi = 0.1 \text{ V/rad}$ (conservative with respect to $P_\mu$), the mixer noise is about $2.5 \times 10^{-16} \text{ rad}^2/\text{Hz}$ ($-156 \text{ dBrad}^2/\text{Hz}$).

There are a number of microwave double-balanced mixers available that exhibit sufficiently low residual flicker. Out of experience, and probably also out of the laziness of keeping our habits, we have a preference for the mixers manufactured by Narda and by Marki. A conservative value for the flicker coefficient
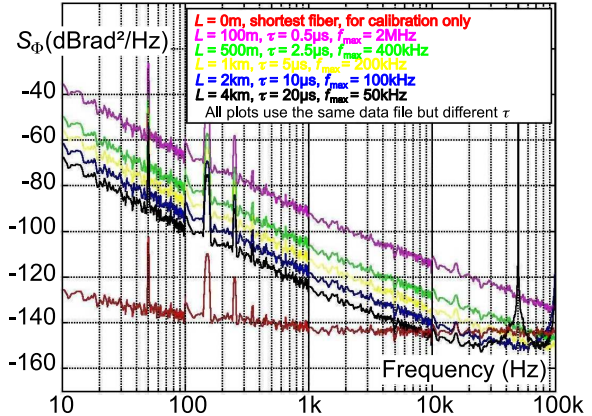


Figure 6: Measured single-channel background noise with zero-length optical fiber.

is $b_{-1} = 10^{-12}$. This makes the mixer noise similar to that of the photodetectors.

Used as a phase detector, the double-balanced mixer needs to be saturated at both inputs. The conversion gain is of 0.1–0.5 V/rad. The power range is of $\pm 5$ dB centered around an optimum power of 5–10 mW. Out of this range, $b_{-1}$ increases. At lower power the conversion gain drops suddenly. This is a consequence of the exponential $i(v)$ characteristics of the internal Schottky diodes.

Mixers are sensitive to the amplitude noise of the input signal. The output voltage $v(t)$ takes the form $v(t) = k_\varphi \varphi(t) + k_\alpha \alpha(t)$, where $\alpha(t)$ is the amplitude fluctuation defined by Eq. (1). This results from the asymmetry of the internal diodes and baluns. In some cases we have measured $k_\varphi/k_\alpha$ as low as 5, while values of 10–20 are common. In photonic systems the contamination from amplitude noise can be a serious problem because of the power fluctuation of some lasers and laser amplifiers. Brendel [28], and later Cibel [29], suggest that the mixer can be operated at a sweet point off the quadrature, where the sensitivity AM noise nulls. A thorough study about the effects of AM noise on phase noise systems [30] shows that the Brendel offset method can not be used in our case. This occurs because the null of amplitude sensitivity results from the equilibrium between equal and opposite sensitivities at the two inputs. The delay line de-correlates the mixer input signals.

## V. EXPERIMENTS

We discuss a number of experiments done with the scheme of Fig. 5 and its variants. Then we assembled a microwave oscillator with the same type of components and we measured its phase noise.

In a first experiment we removed the spools of Fig. 5, replacing them with short optical fibers. At zero fiber length, the oscillator phase noise is not detected. Additionally, the zero delay eliminates at least two noise phenomena, (1) the Rayleigh scattering in the fiber, and (2) the random fluctuation of the
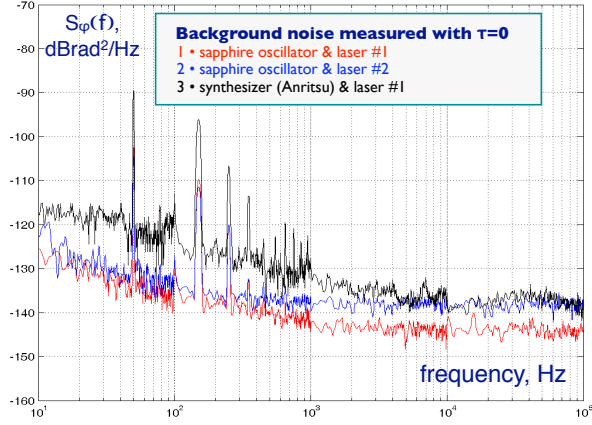
Figure 7: Effect of the laser RIN and of the oscillator-under-test AM noise, measured with zero-length fiber.



Figure 8: Phase noise of a sapphire oscillator.



Figure 9: Background noise, including the optical fibers.

delay due to the laser frequency noise. The latter effect is believed to be negligible. Figure 6 shows the noise of the single channel. The lower curve (red) is the raw phase noise measured by the mixer, accounting for the phase-to-voltage conversion gain from the mixer input to the FFT analyzer. This is $S_\theta(f)$ as defined by Eq. (12)-(13). The other curves are $S_\varphi(f)$ plotted using the same data set $S_\theta(f)$, after unapplying $|H(jf)|^2$ [Eq. (14)] for various fiber lengths. This is the single-channel background noise that we would obtain with a noise-free optical fiber. On Fig. 6, two facts deserve attention. The black curve (4 km fiber, $\tau = 20$ $\mu$s) shows a peak at 50 kHz $1/\tau$ and at 100 kHz $2/\tau$, where unapplying $|H(jf)|^2 = 4\sin^2(\pi f\tau)$ takes a division by zero. Then, the same curve shows two minima 6 dB lower than $S_\theta(f)$ at $f = 25$ kHz and at $f = 75$ kHz, where $|H(jf)|^2 = 4$. The same thing is observed at $f = 50$ kHz on the blue curve (2 km fiber, $\tau = 10$ $\mu$s).

The second experiment shows the effect of the laser RIN and of the AM noise of the oscillator under test, still in single-channel mode with zero-length optical fiber. At zero fiber length, the oscillator phase noise is not detected. The red curve (the lowest) is the same of Fig. 6, measured with the CATV laser, using a 10 GHz sapphire-loaded dielectric-cavity oscillator (for short, sapphire oscillator) operated at room temperature [31]. Besides high stability, the sapphire oscillator performs low AM noise. Replacing the laser with a different one with higher RIN, or replacing the oscillator under test with a synthesizer, the background noise increases significantly.

The third experiment is the phase-noise measurement of a room-temperature sapphire oscillator, still in single-channel mode, with various lengths of the optical fiber. The measured spectra are shown in Fig. 8. Let us focus on the $1/f^3$ noise, which dominates on the figure. When the fiber length is insufficient to detect the noise of the source under test, the plot shows the background noise of the instrument. The background scales with the inverse square length, that is, $-6$ dB in $S_\varphi(f)$ for a factor of 2 in length. This happens with the upper curves (magenta: 100 m length, $\tau = 0.5$ $\mu$s, and red: 500 m
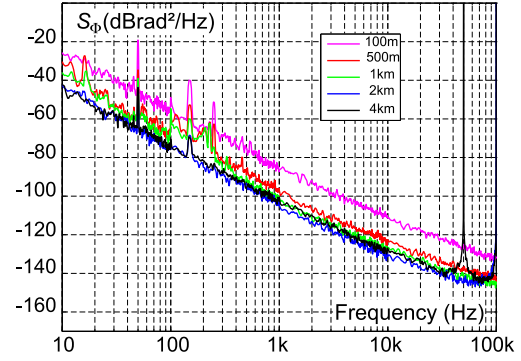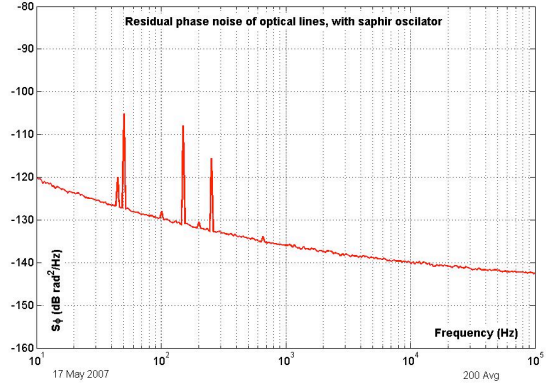
length, $\tau = 2.5$ $\mu$s), which show the background noise of the instrument. Increasing the length, the $1/f^3$ noise no longer decreases (blue: 2 km length, $\tau = 10$ $\mu$s, and black: 4 km length, $\tau = 20$ $\mu$s). This indicates that the instrument measures the phase noise of the sapphire oscillator, still in single-channel mode. To be honest, the sapphire oscillator makes use of a GaAs sustaining amplifier, more noisy than the SiGe amplifier used in the instrument. Nonetheless, this result is a remarkable one because the sapphire oscillator is known as the lowest-noise microwave oscillator.

In a fourth experiment, we measure the noise of the photonic channel using the scheme of Fig. 10. This scheme rejects the noise of the oscillator under test by using two fibers equal in length. This scheme suffers from a number of defects: (1) for practical reasons we can not use the correlation method, (2) we cannot separate the noise of the fibers from the other noises, (3) the $1/f$ noise of the GaAs power amplifiers that drive the EOM might show up. Nonetheless, this scheme has the merit of giving at least an upper bound of the achievable noise. The measured spectrum, shown in Fig. 9, indicates that the $1/f$ phase noise is $b_{-1} = 10^{-11}$ rad$^2$/Hz ($-110$ dBrad$^2$/Hz). At this level, the mixer noise is negligible.

The fifth experiment is the measurement of the dual-channel background noise, with zero-length optical fiber, so that the phase noise of the microwave oscillator is rejected. The spectrum, shown in
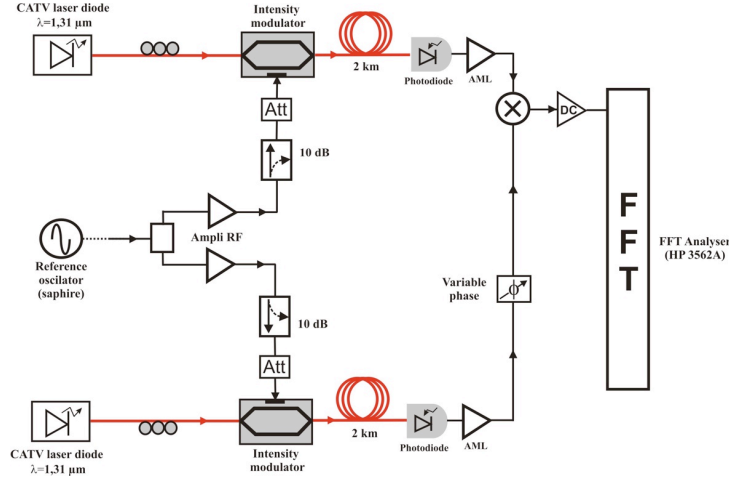
Figure 10: Measurement of the background noise, including the optical fibers.
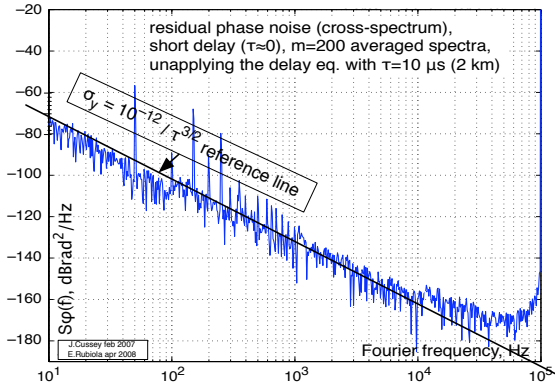


Figure 11: Background noise in two-channel mode, measured with zero-length fiber.
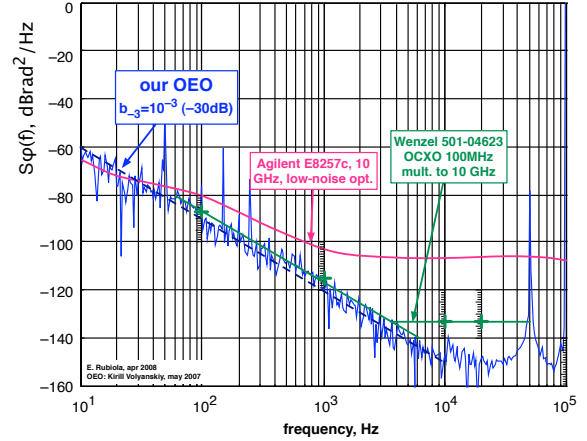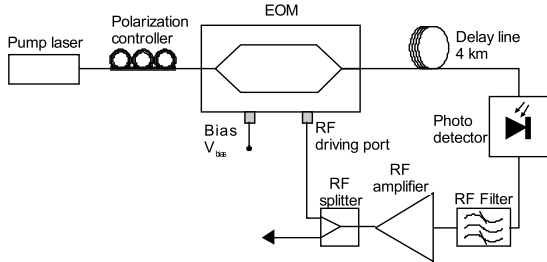


Figure 12: Scheme of the opto-electronic oscillator.



Figure 13: Phase noise of the opto-electronic oscillator.

Fig. 11, is to be taken with some reserve because it does not account for the optical noise phenomena in the fiber. When this experiment was done, the stability of the quadrature condition was insufficient for long acquisitions. For this reason we stopped the measurement after $m = 200$ spectra. This experiment indicates that averaging on 200 spectra the instrument can measure the phase noise of a microwave oscillator having a stability of $10^{-12}$ (floor of the Allan deviation), provided the fibers do not introduce correlated noise in the two channels. The latter assumption seems quite reasonable.

The last experiment is the implementation of an opto-electronic oscillator (Fig. 12) operated at 10 GHz, and the measurement of its phase noise. The amplifier is of the SiGe type, while the photodetector is one of the new units with integrated transconductance amplifier. This makes the microwave chain similar to that of one channel in Fig. 10. In fact, in both cases the chain includes a SiGe amplifier, a GaAs amplifier, and a photodetector. For the flicker noise, the order of the devices in the chain is not relevant at first order. The delay line of the oscillator is 4 km long ($\tau = 20$ $\mu$s). That said, we take the value $b_{-1} = 10^{-11}$ rad$^2$/Hz ($-110$ dBrad$^2$/Hz) as the noise of the optical delay unit, the same of Fig. 9-10, as the noise of the delay line. Though somewhat arbitrary, this value account for the increased length of the fiber (4 km instead of 2 km) and for the photodetector internal amplifier, more noisy than our microwave amplifiers, which compensate the fact that we have one channel instead of two. Feeding $(b_{-1})_{\mathrm{loop}} = 10^{-11}$ rad$^2$/Hz in the oscillator noise theory of Section II D, the expected oscillator frequency flicker is $(b_{-3})_{\mathrm{osc}} = 6.3 \times 10^{-4}$ rad$^2$/Hz ($-32$ dBrad$^2$/Hz). This value is equivalent to a frequency stability of $2.9 \times 10^{-12}$ (floor of the Allan deviation).

The measured noise spectrum (Fig 13) shows a frequency flicker of $10^{-3}$ rad$^2$/Hz ($-30$ dBrad$^2$/Hz), close to the predicted value.

Interestingly, the phase noise of the opto-electronic oscillator is lower than that of one of the lowest-noise microwave synthesizers, and lower than that of a Wenzel quartz oscillator multiplied to 10 GHz. Yet, the frequency of our oscillator can be switched in steps of 50 kHz without degrading the noise.

[1] X. S. Yao and L. Maleki, J. Opt. Soc. Am. B - Opt. Phys. **13**, 1725 (1996).

[2] E. Rubiola, E. Salik, S. Huang, and L. Maleki, J. Opt. Soc. Am. B - Opt. Phys. **22**, 987 (2005), ISSN 0740-3324.

[3] E. Salik, N. Yu, L. Maleki, and E. Rubiola, in *Proc. Europ. Freq. Time Forum and Freq. Control Symp. Joint Meeting* (Montreal, Canada, 2004), pp. 303–306.

[4] P. Salzenstein, J. Cussey, X. Jouvenceau, H. Tavernier, L. Larger, E. Rubiola, and G. Sauvage, Acta Phys. Polonica A **112**, 1107 (2007).

[5] CCIR Study Group VII, in *Standard Frequencies and Time Signals* (International Telecommunication Union (ITU), Geneva, Switzerland, 1990), vol. VII (annex) of *Recommendations and Reports of the CCIR*, pp. 160–171.

[6] H. G. Kimball, ed., *Handbook of selection and use of precise frequency and time systems* (ITU, 1997).

[7] J. Rutman, Proc. IEEE **66**, 1048 (1978).

[8] J. R. Vig (chair.), *IEEE Standard Definitions of Physical Quantities for Fundamental Frequency and Time Metrology–Random Instabilities (IEEE Standard 1139-1999)*, IEEE, New York (1999).

[9] J. Vanier and C. Audoin, *The Quantum Physics of Atomic Frequency Standards* (Adam Hilger, Bristol, UK, 1989), ISBN 0-85274-434-X.

[10] E. Rubiola, in *Proc. 22nd European Frequency and Time Forum* (Toulouse, France, 2008), invited article.

[11] E. Rubiola, *Phase Noise and Frequency Stability in Oscillators* (Cambridge University Press, Cambridge, MA, 2008), ISBN 978-0-521-88677-2, supersedes the abridged version "The Leeson effect," arXiv:physics/0502143. In press.

[12] Y. Kouomou Chembo, K. Volyanskiy, L. Larger, E. Rubiola, and P. Colet, J. Quantum Electron. (2008), Submitted.

[13] D. Eliyahu and L. Maleki, in *Proc. Europ. Freq. Time Forum and Freq. Control Symp. Joint Meeting* (Tampa (FL, USA), 2003), pp. 405–410.

[14] H. T. Friis, Proc. IRE **32**, 419 (1944).

[15] D. Halford, A. E. Wainwright, and J. A. Barnes, in *Proc. Freq. Control Symp.* (1968), pp. 340–341, abstract only is published.

[16] A. Hati, D. Howe, D. Walker, and F. Walls, in *Proc. Europ. Freq. Time Forum and Freq. Control Symp. Joint Meeting* (Tampa, FL, 2003).

[17] F. L. Walls, E. S. Ferre-Pikal, and S. R. Jefferts, IEEE Trans. Ultras. Ferroelec. and Freq. Contr. **44**, 326 (1997).

[18] E. Rubiola and R. Boudot, *$1/f$ noise of RF and microwave amplifiers*, available soon on http://arxiv.org (2008).

[19] R. Boudot, Ph. D. thesis, Université de Franche Comté, Besançon, France (2006).

[20] W. Shieh, X. S. Yao, L. Maleki, and G. Lutes, in *Proc. Optical Fiber Comm. (OFC) Conf.* (San José, CA, 1998), pp. 263–264.

[21] E. Rubiola, E. Salik, N. Yu, and L. Maleki, IEEE Trans. Microw. Theory Tech. **54**, 816 (2006), preprint available on arxiv.org, document arXiv:physics/0503022v1, March 2005.

[22] W. Shieh and L. Maleki, IEEE Photonic Technology Lett. **17**, 474 (2005).

[23] E. Rubiola, V. Giordano, and J. Groslambert, Rev. Sci. Instrum. **70**, 220 (1999), ISSN 0034-6748.

[24] A. Yariv, *Optical Electronics in Modern Communications* (Oxford, New York, NY, 1997), 5th ed.

[25] E. Rubiola and V. Giordano, Rev. Sci. Instrum. **73**, 2445 (2002), also on the web site arxiv.org, document arXiv:physics/0503015v1.

[26] E. Rubiola and V. Giordano, Rev. Sci. Instrum. **71**, 3085 (2000), ISSN 0034-6748.

[27] E. Rubiola and F. Lardet-Vieudrin, Rev. Sci. Instrum. **75**, 1323 (2004), free preprint available on the web site arxiv.org, document arXiv:physics/0503012v1, March 2005.

[28] R. Brendel, G. Marianneau, and J. Ubersfeld, IEEE Trans. Instrum. Meas. **26**, 98 (1977).

[29] G. Cibiel, M. Régis, E. Tournier, and O. Llopis, IEEE Trans. Ultras. Ferroelec. and Freq. Contr. **49**, 784 (2002).

[30] E. Rubiola and R. Boudot, IEEE Trans. Ultras. Ferroelec. and Freq. Contr. **54**, 926 (2007).

[31] V. Giordano, P.-Y. Bourgeois, Y. Gruson, N. Boubekeur, R. Boudot, E. Rubiola, N. Bazin, and Y. Kersalé, Euro. Phys. J. – Appl. Phys. **32**, 133 (2005).